Equilibrium shapes of fluid membranes and carbon nanostructures

Vassil M. Vassilev* e-mail: vasilvas@imbm.bas.bg
Peter A. Djondjorov* e-mail: padjon@imbm.bas.bg
Mariana. Ts. Hadzhilazova** e-mail: murryh@obzor.bio21.bas.bg
Ivailo M. Mladenov** e-mail: mladenov@obzor.bio21.bas.bg
Jan J. Slawianowski*** e-mail: jslawian@ippt.gov.pl

*Institute of Mechanics, BAS
**Institute for Biophysics and Biomedical Engineering, BAS
***Institute of Fundamental Technological Research, PAS

Abstract

The present chapter concerns the continuum modelling of the mechanical behaviour and equilibrium shapes of two types of nano-scale objects: fluid lipid bilayer membranes and carbon nano-structures. A unified continuum model is used to handle four different case studies. Two of them consist in representing in analytic form cylindrical and axisymmetric equilibrium configurations of single-wall carbon nanotubes and fluid lipid bilayer membranes subjected to uniform hydrostatic pressure. The third one is concerned with determination of possible shapes of junctions between a single-wall carbon nanotube and a flat graphene sheet or another single-wall carbon nanotube. The last one deals with the mechanical behaviour of closed fluid lipid bilayer membranes (vesicles) adhering onto a flat homogeneous rigid substrate subjected to micro-injection and uniform hydrostatic pressure.

Keywords: *graphene, carbon nanotubes and nanostructures, junctions, bending energy, natural boundary conditions, cell injection, adhesion, equilibrium shapes*

1. Introduction

This chapter is concerned with the mechanical behaviour and shape analysis of two types of nano-scale objects of quite different physical and chemical nature: fluid membranes (FM's) and carbon nanostructures (CNS's).

Here, by a fluid membrane we mean a membrane formed in aqueous solution by a bilayer of lipid molecules, which are in a fluid state, i.e. the molecules can move freely within the monolayer they belong to. The structure of the bilayer is such that the hydrophobic tails of the lipid molecules situated in different monolayers face one another to form a semi-permeable core, while their hydrophilic heads face the aqueous solutions on either side of the membrane. It is well-known that the lipid bilayer is the main structural component of all biological membranes, the closed lipid bilayer membranes

(vesicles) being thought of as the simplest model systems for studying basic physical properties of the more complex biological cells.

By a carbon nanostructure we mean any stable configuration of the curved (bended and/or stretched) graphene such as: carbon nanotubes (CNT's), nano-horns, nanotori, fullerenes, wormholes, schwartzites and so on. Some of these structures (especially CNT's) are utilized as basic ingredients of nano-structured materials, such as nanotube-based nanocomposites or functionalized CNT membranes used in water desalination, for instance. Others are basic building blocks of nanoelectromechanical systems (NEMS), nanosensors and other nano-devices.

The underlying idea behind the present contribution is to combine the study of the mechanical behaviour of FM's and CNS's on the bases of a unified continuum mechanics model. In this way, we hope to achieve a significant transfer of knowledge between FM and CNS sciences and thus to accelerate the development of both fields.

The idea for such a unification emerges in a natural way when one compares the known configurations of FM's and CNS's and realizes that their shapes are similar. This similarity is not accidental. It is intimately connected with the following observations:

a) regardless of the particular chemical or physical structure, the geometry of both the foregoing types of objects is essentially two-dimensional and therefore it can be described in terms of the differential geometry of surfaces;

b) both types of the considered objects exhibit elastic behaviour within a large scale, their elastic properties being characterized (in the simplest models) by a few parameters, and hence there is a good reason to believe that the fundamental principles of the two-dimensional elasticity are potentially applicable for the description of their mechanical behaviour;

c) usually the equilibrium configurations observed in the nature can be viewed as local extrema of appropriate variational functionals subjected to various constraints and boundary conditions.

To summarize, in the case of a curved two-dimensional elastic continuum, such as that required for FM's and CNS's according to the aforementioned observations **a)** – **c)**, the geometry of the deformed atomic or molecular lattice is expressed in terms of the invariants of the strain (first fundamental form) and curvature (second fundamental form) of a surface embedded in the three-dimensional Euclidean space, which is supposed to provide a local extremum of an appropriate energy functional subjected to certain constraints and boundary conditions.

The problems envisaged to be addressed in this article are concerned with the analytic description of cylindrical and axisymmetric equilibrium shapes of FM's and CNT's under uniform hydrostatic pressure, determination of junctions of CNT's to a flat graphene sheet or to other CNT's, deformation of cell membranes subjected to micro-injection and adhesion of injected vesicles to flat rigid surfaces.

2. Modelling

2.1 Continuum modelling of the equilibrium shapes of FM's

The foundation of the current theoretical understanding of the shapes and

mechanical response of fluid membranes to different types of excitations can be traced more than thirty years back (see, e.g., [1–3]) to the works by Canham [4] and Helfrich [5] in which the first one of the so-called curvature models was introduced and developed.

Besides, two other curvature models have also been developed. The first one, referred to as the bilayer-couple model, was suggested by Svetina and Žekš in [6] on the ground of the bilayer-couple hypothesis [7]. The second one is known as the area-difference-elasticity model [8–10]. In all models of this kind, the vesicle's membrane is regarded as a two-dimensional surface $\mathcal{S}$ embedded in the three-dimensional Euclidean space and assumed to exhibit purely elastic behaviour (elastic bending without stretching) described in terms of its mean H and Gaussian K curvatures, and two material constants associated with the bending rigidity of the membrane.

Within the Helfrich spontaneous curvature model [5], the two-dimensional surface $\mathcal{S}$ representing a fluid membrane in equilibrium is assumed to provide a local extremum of the elastic bending energy functional

$$\mathcal{F}_b = \frac{k_c}{2}\int_{\mathcal{S}}\left(2H + c_0\right)^2 \mathrm{d}A + k_G\int_{\mathcal{S}} K\mathrm{d}A$$

under the constraints of fixed total membrane area A and enclosed volume V (if the membrane is subjected to a uniform hydrostatic pressure p). This functional is also called curvature or shape energy. Here c_0, k_c and k_G are three real constants representing the spontaneous curvature (a constant introduced by Helfrich to reflect a possible asymmetry of the membrane or its environment), bending and Gaussian rigidity of the membrane, respectively.

Using two Lagrange multipliers λ and p to take into account the aforementioned constraints, this yields the functional

$$\mathcal{F}_{bc} = \frac{k_c}{2}\int_{\mathcal{S}}\left(2H + c_0\right)^2 \mathrm{d}A + k_G\int_{\mathcal{S}} K\mathrm{d}A + \lambda\int_{\mathcal{S}}\mathrm{d}A + p\int\mathrm{d}V.$$

The Lagrange multiplier λ corresponds to the constraint of fixed total area and can be interpreted as the tensile stress or chemical potential associated with the number of the lipid molecules located at the membrane surface, while the pressure p appearing as another Lagrange multiplier corresponds to the constraint of fixed enclosed volume V.

The Euler-Lagrange equation associated with the functional $\mathcal{F}_{bc}$, which is often referred to as the membrane shape equation, is derived by Ou-Yang and Helfrich in [11] and reads

$$\Delta H + \left(2H + c_0\right)\left(H^2 - \frac{c_0}{2}H - K\right) - \frac{\lambda}{k_c}H = -\frac{p}{2k_c}, \qquad (1)$$

where Δ is the Laplace-Beltrami operator on the surface $\mathcal{S}$. It is worth noting that the second term in the bending energy $\mathcal{F}_b$ does not effect equation (1) since its contribution to the overall Lagrangian density is a total divergence as follows from the Liouville's form of Gauss's Theorema Egregium (see, e.g., [12]). Actually, for closed membranes without edges the integral over the Gaussian curvature K is a topological invariant by virtue of the Gauss-Bonnet theorem and therefore it may be disregarded until the

topology of the membrane remains unchanged. This term, however, plays an important role in the theory of fluid membranes with free edges (cf. [13–15]). It is worth noting also that in the case $\lambda = p = c_0 = 0$, equation (1) determines the so-called Willmore surfaces [16], which are of great interest for the conformal geometry.

Let us remark also that both spontaneous curvature and bilayer-couple models lead to the same shape equation as pointed out by Svetina and Žekš in [6]. The same holds true for the area-difference-elasticity model, see [17].

The study of the equilibrium shapes of fluid membranes and the response of the latter to a uniform hydrostatic pressure and other types of excitations has attracted much attention in the past few decades due to the importance of this kind of research in biology and medicine. It should be noted that only a few exact analytic solutions to the shape equation (1) have been reported so far, which is not quite a surprise since this is a highly nonlinear partial differential equation. These are solutions determining: circular cylinders and spheres [11], circular biconcave discoids [21, 22], Clifford tori [18–20], Delaunay surfaces [23–25], nodoidlike and unduloidlike shapes [25], Dupin cyclides [2], several types of Willmore [16, 26] and constant squared mean curvature density surfaces [27], as well as cylindrical surfaces [2, 28, 29]. It should be noted, however, that leaving aside spheres, circular cylinders, Dupin cyclides and tori whose parametric equations are well known for many years, to the best of our knowledge explicit parametrizations of the rest of the foregoing surfaces are missing except for the Delaunay [23, 24], unduloidlike [30] and cylindrical surfaces [29].

2.2 Continuum modelling of the equilibrium shapes of CNS's

Nowadays, it is a common opinion among the scientists that the onset of the "carbon nano-research" was set by Kroto *et al.* [31] in 1985. Peculiar carbon nano-structures were reported before 1985 (see [32–34]), but Kroto *et al.* [31] were the first who pointed out some extraordinary properties of the C_{60} fullerene – its remarkable stability and symmetry. It is this feature that attracted the attention of the scientific community to CNS's and, since that time, the number of discovered CNS's is rapidly increasing, an important milestone in this story being the experimental observation of carbon nanotubes by Iijima [35] in 1991. Today, one can find a vast amount of research articles by scientists from mathematics, chemistry, physics, as well as from interdisciplinary areas such as material science, nanotechnology, etc., in which the mechanical, electrical, optical, etc. properties of CNS's are studied. As a consequence, materials, devices and technologies based on CNS's are now distributed in a wide variety of human activities.

Shortly after the experimental discovery of multi-wall [35] and single-wall [36,37] carbon nanotubes and the reported progress in their large-scale synthesis [38], a remarkable mechanical behaviour of this carbon alotrops was observed. The findings provided by high-resolution transmission electron microscopy [39–42] demonstrated that these nanostructures can sustain large deformations of their initial circular-cylindrical shape without occurrence of irreversible atomic lattice defects. As noticed in [41]: "*Thus, within a wide range of bending, the tube retains an all-hexagonal structure and reversibly returns to its initial straight geometry upon removal of the bending force*."

One of the most widely used approaches for determining the mechanical response of CNS's is the molecular dynamic simulation. Within this approach, a CNS is considered as a multibody system in which the interaction of a given atom with the neighbouring ones is regarded. The energy of this interaction is modelled through certain empirical interatomic potentials. In 1988, Tersoff [43] suggested a general approach for derivation of such potentials and applied it to silicon. In 1990, Brenner [44] adapted and modified Tersoff's results and suggested an interatomic potential for carbon atomic bonds. Another potential of such kind was introduced in 1992 by Lenosky *et al.* [45].

On the other hand, the observed elastic behaviour of the carbon nanotubes, their essentially two-dimensional atomic lattice structure and the intrinsic hexagonal symmetry of the latter gave firm arguments to Yakobson *et al.* [46] to develop a continuum mechanics approach, based on the classical theory of isotropic thin elastic shells [47], for explanation of the mechanical properties and exploration of the deformed configurations of these carbon molecules.

The advantage of such an approach, in comparison with the ones based directly on the interatomic interactions, is that the continuum mechanics models are amenable to analytical calculations and allow efficient numeric simulations. Therefore, it is not surprising that since the pioneering work [46], the application of continuum mechanics to the study of mechanical behaviour of carbon nano-structures has become common practice although, as noted in [46]: "*its relevance for a covalent-bonded system of only a few atoms in diameter is far from obvious*".

The easiest way of introducing a continuum model of the regarded type of atomistic systems is to emulate the basic idea of the work by Yakobson *et al.* [46], that is to adopt a standard continuum theory (some of the well-known shell theories [48–50], for instance) and to adjust the material parameters (such as Young's modulus, Poisson's ratio, bending rigidity, shell thickness, etc.) to the data available by atomistic simulations. This approach has been used by various authors (see, e.g., [51–55]) and turned out to be quite successful.

Actually, even without explicitly formulating a consistent theory, recourse to continuum and structural mechanics concepts, such as those mentioned above is ubiquitous in the nanotube literature (see, e.g., [56–58]).

The more sophisticated attempts at deriving continuum theories for CNS's incorporate the specific atomic lattice structure and use interatomic interaction potentials of Tersoff-Brenner [43, 44, 59] or Lenosky [45] type, for instance. The essential idea behind this kind of theories is to express the deformation of the atomic lattice in terms of the geometric quantities characterizing the deformation of the continuum using an appropriate continuum limit [60–62] or kinematic assumption, such as the Cauchy-Born rule or some of its modifications [63–69].

In the case of a curved two-dimensional continuum, such as that required within the continuum modelling of the carbon nanostructures, the geometry of the deformed lattice is expressed in terms of the invariants of the strain (first fundamental form) and curvature (second fundamental form) of the deformed surface.

In what follows, we have adopted the continuum theory developed by Ou-Yang *et al.* in [60–62], which is based on the continuum limit of the Lenosky potential [45], an extra term being added to the corresponding deformation energy to take into account the

screw dislocation core-like deformation, as it was suggested by Xie *et al.* in [70].

According to Lenosky *et al.* [45], the deformation energy of a single layer of curved graphite carbon has the form

$$\mathcal{F} = \varepsilon_0 \sum_{(ij)} \frac{1}{2}\left(r_{ij} - r_0\right)^2 + \varepsilon_1 \sum_i \left(\sum_{(j)} \mathbf{u}_{ij} \right)^2 + \varepsilon_2 \sum_{(ij)} \left(1 - \mathbf{n}_i \cdot \mathbf{n}_j\right)^2 + \varepsilon_3 \sum_{(ij)} \left(\mathbf{n}_i \cdot \mathbf{u}_{ij}\right)\left(\mathbf{n}_j \cdot \mathbf{u}_{ji}\right),$$

where r_{ij} is the bond length between atoms i and j after deformation; r_0 is the initial bond length of planar graphite; $\mathbf{u}_{ij}$ is a unit vector pointing from carbon atom i to its neighbor j; $\mathbf{n}_i$ is a unit vector normal to the plane determined by the three neighbors of atom i; ε_0, ε_1, ε_2 and ε_3 are the so-called bond-bending parameters. The summation $\sum_{(j)}$ is taken over the three nearest-neighbour atoms j to i atom and $\sum_{(ij)}$ is taken over all nearest-neighbor atoms.

The continuum limit of the Lenosky potential $\mathcal{F}$ yields the following expression for the deformation energy [61]

$$\mathcal{F}_{cl} = \int_{\mathcal{S}} \left[\frac{k_c}{2}(2H)^2 + k_G K + \frac{k_d}{2}(2J)^2 + \tilde{k} Q \right] \mathrm{d}A,$$

where $\mathcal{S}$ is the deformed surface; H and K are its mean and Gaussian curvatures; $\mathrm{d}A$ is the area element on the surface $\mathcal{S}$; J and Q are the first and second invariants of the in-plane deformation tensor, which are often referred to as the "mean" and "Gaussian" strains, respectively, and the constants k_c, k_G, k_d and $\tilde{k}$ are given through the bond-bending parameters ε_0, ε_1, ε_2 and ε_3 by the expressions

$$k_c = \frac{r_0^2}{32\Omega}(18\varepsilon_1 + 24\varepsilon_2 + 9\varepsilon_3), \qquad k_G = -k_c \frac{8\varepsilon_2 + 3\varepsilon_3}{(6\varepsilon_1 + 8\varepsilon_2 + 3\varepsilon_3)},$$

$$k_d = \frac{9}{16\Omega}(\varepsilon_0 r_0^2 + \varepsilon_1), \qquad \tilde{k} = -\frac{3}{8\Omega}(\varepsilon_0 r_0^2 + 3\varepsilon_1),$$

where $\Omega = 3\sqrt{3}r_0^2/4$ is the occupied area per atom.

The values of the parameters ε_1, ε_2 and ε_3 were determined by Lenosky *et al.* [45] through a local density approximation, while the value of the parameter ε_0 was obtained by Zhou *et al.* in [71, 72] from the force-constant method. In both cases, it is assumed that $r_0 = 1.42$ Å. These values are

$$\varepsilon_0 = 57\mathrm{eV/Å}^2, \qquad \varepsilon_1 = 0.96\mathrm{eV}, \qquad \varepsilon_2 = 1.29\mathrm{eV}, \qquad \varepsilon_3 = 0.05\mathrm{eV},$$

and consequently

$$k_c = 1.17\mathrm{eV}, \qquad k_G = -0.75\mathrm{eV},$$

$$k_d = 24.88\text{eV/Å}^2, \qquad \widetilde{k} = 16.87\text{eV/Å}^2.$$

Recently, Tu and Ou-Yang [62] have revised the Lenosky potential in order to take into account that the energy costs due to the in-plane and out-of plane bond angle changes are quite different. In continuum limit, they have obtained the same expression for curvature energy $\mathcal{F}_{cl}$, but now

$$k_c = 1.62\text{eV}, \qquad k_G = -0.72\text{eV},$$
$$k_d = 22.97\text{eV/Å}^2, \qquad \widetilde{k} = 19.19\text{eV/Å}^2,$$

$r_0 = 1.41$ Å being the result for the initial bond length of planar graphite. These "material" parameters and the functional $\mathcal{F}_{cl}$ describe the deformation of a single-wall carbon nanotube as that of a two-dimensional isotropic elastic continuous media.

Actually, the last two terms in the functional $\mathcal{F}_{cl}$ accounting for the in-plane deformation can be neglected since the contribution of the bond stretching to the deformation energy is less than 1%, see [45]. Instead of this, the graphene sheet can be assumed to be inextensible under the bending related to the remaining two terms in the functional $\mathcal{F}_{cl}$. If, in addition, it is assumed that a uniform hydrostatic pressure p is applied and the term accounting for the screw dislocation core-like deformation suggested in [70] is included, one arrives at the conclusion that the equilibrium shapes of a single-wall carbon nanotube are determined, just as for a fluid membrane, by the extremals of the functional $\mathcal{F}_{bc}$ in which, of course, the meaning and values of the constant k_c, k_G, and c_0 are different.

To summarize, the extremals of the functional $\mathcal{F}_{bc}$ determined by the corresponding Euler-Lagrange equation (1), that is the membrane shape equation, provide a unified continuum model for studying the equilibrium shapes of both FM's and CNS's subjected to uniform hydrostatic pressure. Of course, one should be aware that this model accounts for elastic bending only, the effects of the in-plane stretching being neglected.

2.3 Shape equation for cylindrical FM's and CNS's

Consider a cylindrical surfaces $\mathcal{S}$ whose directrix is a plane curve Γ, which is parametrized by its arclength s, the corresponding generatrix being perpendicular to the plane the directrix Γ lies in (see Figure 1). For such a surface the shape equation (1) reduces to the ordinary differential equation

$$\frac{\mathrm{d}^2\kappa}{\mathrm{d}s^2} + \frac{1}{2}\kappa^3(s) - \mu\kappa(s) - \sigma = 0, \tag{2}$$

where $\sigma = -p/k_c$, $\mu = c_0^2/2 + \lambda/k_c$ and $\kappa(s)$ is the curvature of the curve Γ.

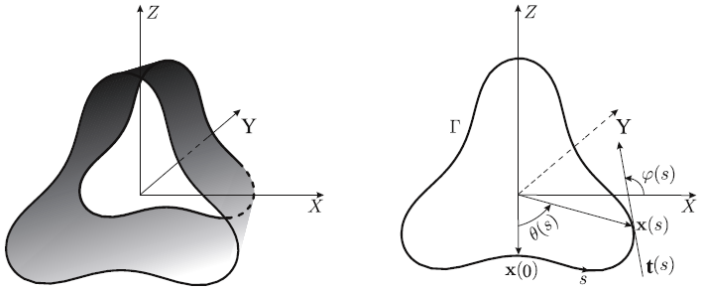

Figure 1. A slice of the infinite generalized cylinder (left) and its intersection with the plane $Y \equiv 0$ (right). Here, $\mathbf{t}(s)$, $\varphi(s)$ and $\theta(s)$ are the tangent vector, slope angle and the angle between the position vectors $\mathbf{x}(0)$ and $\mathbf{x}(s)$, respectively.

Indeed, using the standard formulas from the textbooks on classical differential geometry (e.g., [12]) one can easily find that for a cylindrical surface parametrized in the above way $H = (1/2)\kappa(s)$, $\Delta H = (1/2)\mathrm{d}^2\kappa(s)/\mathrm{d}s^2$ and $K = 0$. Substituting the latter expressions in equation (1) one immediately obtains Eq. (2).

Evidently, Eq. (2) possesses the following first integral

$$\left(\frac{\mathrm{d}\kappa}{\mathrm{d}s}\right)^2 = P(\kappa), \qquad P(\kappa) = -\frac{1}{4}\kappa^4 + \mu\kappa^2 + 2\sigma\kappa + \varepsilon, \tag{3}$$

where ε is an arbitrary real constant of integration, which allows its solutions to be expressed in analytic form by means of the roots of the polynomial $P(\kappa)$, see [29, 73].

Then, using the geometrical relations

$$\frac{\mathrm{d}\varphi(s)}{\mathrm{d}s} = \kappa(s), \qquad \frac{\mathrm{d}x}{\mathrm{d}s} = \cos\varphi(s), \qquad \frac{\mathrm{d}z}{\mathrm{d}s} = \sin\varphi(s) \tag{4}$$

where $\varphi(s)$ is the tangent (slope) angle while $x(s)$ and $z(s)$ are the components of the position vector $\mathbf{x}(s)$ of the curve Γ with respect to a certain rectangular Cartesian coordinate frame in the Euclidean plane, i.e., $\mathbf{x}(s) = x(s)\mathbf{i} + z(s)\mathbf{j}$, where $\mathbf{i}$ and $\mathbf{j}$ are the unit vectors along the coordinate axes x and z, respectively (see Figure 1), one can restore the curve (up to a rigid motion in the plane) expressing its parametric equations by the quadratures

$$x(s) = \int \cos(\varphi(s))\mathrm{d}s, \qquad z(s) = \int \sin(\varphi(s))\mathrm{d}s \tag{5}$$

where

$$\varphi(s) = \int \kappa(s)\mathrm{d}s. \tag{6}$$

2.4 Shape equation for axisymmetric FM's and CNS's

An axisymmetric FM or CNS will be thought of as a surface of revolution obtained

by revolving around the Z-axis a plane curve Γ laying in the XOZ-plane (see Figure 2) usually referred to as its profile curve.

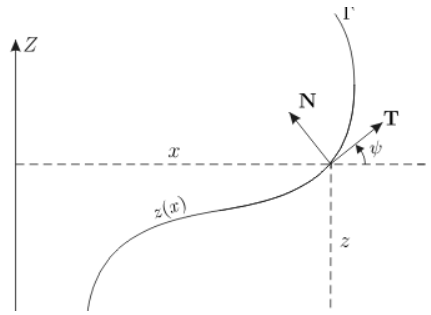

Figure 2. Geometry of the profile curve.

If s denotes the arclength along the curve Γ, $x(s)$ and $z(s)$ are the components of the position vector $\mathbf{x}(s) = \big(x(s), z(s)\big)$ of the curve Γ (see Figure 2) and $\psi(s)$ denotes the slope of the tangent to the curve with respect to the OX axis measured counterclockwise, one has the following geometrical relations

$$\frac{\mathrm{d}\psi(s)}{\mathrm{d}s} = \kappa(s), \qquad \frac{\mathrm{d}x}{\mathrm{d}s} = \cos\psi(s), \qquad \frac{\mathrm{d}z}{\mathrm{d}s} = \sin\psi(s) \tag{7}$$

which can be deduced either from Figure 2, or using the Frenet-Serret equations

$$\frac{\mathrm{d}\mathbf{x}(s)}{\mathrm{d}s} = \mathbf{T}(s), \qquad \frac{\mathrm{d}\mathbf{T}}{\mathrm{d}s} = \kappa\mathbf{N}, \qquad \frac{\mathrm{d}\mathbf{N}}{\mathrm{d}s} = -\kappa\mathbf{T} \tag{8}$$

in which **T** and **N** are the unit tangent and the inward unit normal vectors to the curve, respectively, and $\kappa(s)$ is its curvature.

To obtain the shape equation for axisymmetric FM's and CNS's, one can represent the profile curve Γ by the graph $(x, z(x))$ of the function $z = z(x)$ (see Figure 2) and in this case the general shape equation (1) reduces to the following nonlinear third-order ordinary differential equation

$$\begin{aligned}\cos^3\psi\frac{\mathrm{d}^3\psi}{\mathrm{d}x^3} = {} & 4\sin\psi\cos^2\psi\frac{\mathrm{d}^2\psi}{\mathrm{d}x^2}\frac{\mathrm{d}\psi}{\mathrm{d}x} - \cos\psi\left(\sin^2\psi - \frac{1}{2}\cos^2\psi\right)\left(\frac{\mathrm{d}\psi}{\mathrm{d}x}\right)^3 \\ & + \frac{7\sin\psi\cos^2\psi}{2x}\left(\frac{\mathrm{d}\psi}{\mathrm{d}x}\right)^2 - \frac{2\cos^3\psi}{x}\frac{\mathrm{d}^2\psi}{\mathrm{d}x^2} \\ & + \left(\frac{\lambda}{k_c} + \frac{c_0^2}{2} - \frac{2c_0\sin\psi}{x} - \frac{\sin^2\psi - 2\cos^2\psi}{2x^2}\right)\cos\psi\frac{\mathrm{d}\psi}{\mathrm{d}x}\end{aligned} \tag{9}$$

$$+\left(\frac{\lambda}{k_c}+\frac{c_0^2}{2}-\frac{\sin^2\psi+2\cos^2\psi}{2x^2}\right)\frac{\sin\psi}{x}-\frac{p}{k_c}$$

(derived by Hu and Ou-Yang in [20]) where ψ is again the angle between the *X*-axis and the tangent vector **T** but now considered as a function of the variable x.

Going back to the arclength variable s, one can, using the second one of relations (7), rewrite Eq. (9) in the form

$$\begin{aligned}&\frac{\mathrm{d}^3\psi}{\mathrm{d}s^3}+\frac{2\cos\psi}{x}\frac{\mathrm{d}^2\psi}{\mathrm{d}s^2}+\frac{1}{2}\left(\frac{\mathrm{d}\psi}{\mathrm{d}s}\right)^3-\frac{3\sin\psi}{2x}\left(\frac{\mathrm{d}\psi}{\mathrm{d}s}\right)^2\\&\quad+\left(\frac{1-3\cos^2\psi}{2x^2}+\frac{2c_0}{x}\sin\psi-\frac{1}{2}c_0^2-\lambda\right)\frac{\mathrm{d}\psi}{\mathrm{d}s}\\&\quad+\left(\frac{1+\cos^2\psi}{2x^2}-\frac{1}{2}c_0^2-\lambda\right)\frac{1}{x}\sin\psi=p.\end{aligned}\tag{10}$$

Alternatively, following the approach first used by Seifert *et al.* [74], one can start directly from the bending energy functional $\mathcal{F}_b$, which in the case of an axisymmetric surface takes the form

$$\mathcal{A}=2\pi k_c\int_0^L\frac{1}{2}\left(\frac{\mathrm{d}\psi}{\mathrm{d}s}+\frac{\sin\psi}{x}+c_0\right)^2 x\mathrm{d}s+2\pi k_G\int_0^L\frac{\mathrm{d}\psi}{\mathrm{d}s}\sin\psi\mathrm{d}s,$$

where L is the total length of the profile curve, since the mean H and Gaussian K curvatures of a surface in revolution are given by the expressions

$$H=\frac{1}{2}\left(\frac{\mathrm{d}\psi}{\mathrm{d}s}+\frac{\sin\psi}{x}\right),\qquad K=\frac{\mathrm{d}\psi}{\mathrm{d}s}\frac{\sin\psi}{x}.$$

Then, taking into account the work done by the hydrostatic pressure p, the constraint of fixed total area of the membrane and the geometric relations $(7)_2$, $(7)_3$ by introducing three Lagrange multipliers $\lambda(s)$, $\mu(s)$, $\eta(s)$ and an auxiliary function $\alpha(s)$ such that $\alpha(L)-\alpha(0)=A_0/2\pi$, where A_0 is a certain fixed value of the total area of the membrane, one arrives at the functional

$$\mathcal{A}_c=2\pi k_c\int_0^L\mathcal{L}\mathrm{d}s$$

whose Lagrangian density $\mathcal{L}$ is given by the expression

$$\begin{aligned}\mathcal{L}=\;&\frac{1}{2}\left(\frac{\mathrm{d}\psi}{\mathrm{d}s}+\frac{\sin\psi}{x}+c_0\right)^2 x+\frac{k_G}{k_c}\frac{\mathrm{d}\psi}{\mathrm{d}s}\sin\psi+\frac{P}{3}x\left(x\frac{\mathrm{d}z}{\mathrm{d}s}-z\frac{\mathrm{d}x}{\mathrm{d}s}\right)\\&+\lambda\left(\frac{\mathrm{d}\alpha}{\mathrm{d}s}-x\right)+\mu\left(\frac{\mathrm{d}x}{\mathrm{d}s}-\cos\psi\right)+\eta\left(\frac{\mathrm{d}z}{\mathrm{d}s}-\sin\psi\right)\end{aligned}\tag{11}$$

where $P=p/k_c$. Next, setting to zero the first variation of the functional $\mathcal{A}$ one obtains the following system of Euler-Lagrange equations

$$\begin{aligned}
\frac{\mathrm{d}^2\psi}{\mathrm{d}s^2} &= -\frac{\mathrm{d}\psi}{\mathrm{d}s}\frac{\cos\psi}{x} + \frac{\sin 2\psi}{2x^2} + \mu\frac{\sin\psi}{x} - \eta\frac{\cos\psi}{x} \\
\frac{\mathrm{d}\mu}{\mathrm{d}s} &= \frac{1}{2}\left(\frac{\mathrm{d}\psi}{\mathrm{d}s} + c_0\right)^2 - \frac{1}{2}\left(\frac{\sin\psi}{x}\right)^2 - \lambda + Px\sin\psi, \\
\frac{\mathrm{d}\eta}{\mathrm{d}s} &= -Px\cos\psi, \qquad \frac{\mathrm{d}\alpha}{\mathrm{d}s} = x, \qquad \frac{\mathrm{d}\lambda}{\mathrm{d}s} = 0, \\
\frac{\mathrm{d}x}{\mathrm{d}s} &= \cos\psi, \qquad \frac{\mathrm{d}z}{\mathrm{d}s} = \sin\psi
\end{aligned} \tag{12}$$

and natural boundary conditions

$$\left[\hat{M}\delta\psi + \lambda\delta\alpha + \hat{\mu}\delta x + \hat{\eta}\delta z + \mathcal{H}\delta s\right]_0^L = 0, \tag{13}$$

where

$$\hat{M} = \left[\frac{\mathrm{d}\psi}{\mathrm{d}s} + \left(1 + \frac{k_G}{k_c}\right)\frac{\sin\psi}{x} + c_0\right]x, \tag{14}$$

$$\hat{\mu} = \mu - \frac{1}{3}Pxz, \qquad \hat{\eta} = \eta + \frac{1}{3}Px^2, \tag{15}$$

$$\mathcal{H} = \frac{1}{2}\left[\left(\frac{\mathrm{d}\psi}{\mathrm{d}s}\right)^2 - \left(\frac{\sin\psi}{x} + c_0\right)^2\right]x + \lambda x + \mu\cos\psi + \eta\sin\psi. \tag{16}$$

Actually, $\mathcal{H}$ is a conserved quantity on the smooth solutions of the Euler-Lagrange equations (12) due to the invariance of the functional $\mathcal{A}_c$ under the translations of the independent variable s. In [75], Jülicher and Seifert show that $\mathcal{H} = 0$ is the necessary and sufficient condition for the shape equations (12) and (10) to be equivalent. Therefore, henceforward we assume $\mathcal{H} = 0$. Moreover, $\lambda(L)\delta\alpha(L) - \lambda(0)\delta\alpha(0) = 0$ because of the constraint of fixed total area and the fact that λ turned out to be a constant. Therefore the natural boundary conditions (13) change to

$$\left[\hat{M}\delta\psi + \hat{\mu}\delta x + \hat{\eta}\delta z\right]_0^L = 0. \tag{17}$$

The variations of the functions ψ, x and z at the contours C_0 and C_L corresponding to the values $s = 0$ and $s = L$ of the arclength variable s remain to be specified in a suitable manner depending on the particular problem considered.

Observing the natural boundary conditions (17), one can immediately interpret

$$M = 2\pi k_c \hat{M} \tag{18}$$

and

$$\mathbf{F} = 2\pi k_c \hat{\mathbf{F}}, \qquad \hat{\mathbf{F}} = \hat{\mu}\mathbf{i} + \hat{\eta}\mathbf{j} \tag{19}$$

where $\mathbf{i}$ and $\mathbf{j}$ denote the unit vectors along the coordinate axes X and Z, as the bending moment (couple resultant) and force (stress resultant) at any contour of the membrane.

3 Case studies

3.1 Cylindrical equilibrium shapes of FM's and CNT's under pressure

The aim of this Section is to give, following [29, 73, 76], an exhaustive analytic description of the cylindrical equilibrium shapes of FM's and CNT's subjected to uniform hydrostatic pressure, i.e., to present all solutions of the membrane shape equation (2) determining such shapes, together with the expressions for the corresponding position vectors, in explicit analytic form.

For that purpose, we are interested in real-valued solutions $\kappa(s) \neq \text{const}$ of equation (2) possessing smooth derivatives, which give rise to closed non-self-intersecting (simple) curves Γ. Once such a solution is known, it is possible to find the components $x(s)$ and $z(s)$ of the position vector $\mathbf{x}(s) = x(s)\mathbf{i} + y(s)\mathbf{j}$, of the corresponding directrix Γ (up to a rigid motion in the plane XOZ) in the standard manner using quadratures (5) and (6). However, in what follows we will show that the specific differential structure of equation (2) allows to express the components of the position vector in terms of the curvature $\kappa(s)$, its derivative $\mathrm{d}\kappa(s)/\mathrm{d}s$ and its integral, that is the slope angle $\varphi(s)$, as follows

$$\begin{aligned} x(s) &= \frac{1}{\sigma}\frac{\mathrm{d}\kappa(s)}{\mathrm{d}s}\cos\varphi(s) + \frac{1}{2\sigma}(\kappa^2(s) - 2\mu)\sin\varphi(s), \\ z(s) &= \frac{1}{\sigma}\frac{\mathrm{d}\kappa(s)}{\mathrm{d}s}\sin\varphi(s) - \frac{1}{2\sigma}(\kappa^2(s) - 2\mu)\cos\varphi(s). \end{aligned} \tag{20}$$

First, let us recall that the unit tangent vector $\mathbf{t}(s)$ and the unit inward normal vector $\mathbf{n}(s)$ to the curve Γ are given as follows

$$\mathbf{t}(s) = \frac{\mathrm{d}\mathbf{x}(s)}{\mathrm{d}s} = \frac{\mathrm{d}x}{\mathrm{d}s}\mathbf{i} + \frac{\mathrm{d}y}{\mathrm{d}s}\mathbf{j}, \qquad \mathbf{n}(s) = -\frac{\mathrm{d}y}{\mathrm{d}s}\mathbf{i} + \frac{\mathrm{d}x}{\mathrm{d}s}\mathbf{j} \tag{21}$$

and are related to the curvature $\kappa(s)$ of the curve Γ through the Frenet-Serret formulas [12]

$$\frac{\mathrm{d}\mathbf{t}(s)}{\mathrm{d}s} = \kappa(s)\mathbf{n}(s), \qquad \frac{\mathrm{d}\mathbf{n}(s)}{\mathrm{d}s} = -\kappa(s)\mathbf{t}(s). \tag{22}$$

Then, using formulas (21), one can show by a direct computation that the following identity holds

$$\begin{aligned} &\frac{\mathrm{d}}{\mathrm{d}s}\left(\frac{\mathrm{d}\kappa(s)}{\mathrm{d}s}\mathbf{t}(s) - \frac{1}{2}(\kappa^2(s) - 2\mu)\mathbf{n}(s) - \sigma\mathbf{x}(s)\right) \\ &= \left(\frac{\mathrm{d}^2\kappa(s)}{\mathrm{d}s^2} + \frac{1}{2}\kappa^3(s) - \mu\kappa(s) - \sigma\right)\mathbf{t}(s) + \frac{\mathrm{d}\kappa(s)}{\mathrm{d}s}\left(\frac{\mathrm{d}\mathbf{t}(s)}{\mathrm{d}s} - \kappa(s)\mathbf{n}(s)\right) \\ &- \frac{1}{2}(\kappa^2(s) - 2\mu)\left(\frac{\mathrm{d}\mathbf{n}(s)}{\mathrm{d}s} + \kappa(s)\mathbf{t}(s)\right). \end{aligned} \tag{23}$$

Hence, taking into account the Frenet-Serret formulas (22), one can represent the position

vector $\mathbf{x}(s)$ of a plane curve of curvature $\kappa(s)$ in the form

$$\mathbf{x}(s)=\frac{1}{\sigma}\frac{\mathrm{d}\kappa(s)}{\mathrm{d}s}\mathbf{t}(s)-\frac{1}{2\sigma}(\kappa^2(s)-2\mu)\mathbf{n}(s)+\mathbf{C}$$

where $\mathbf{C}$ is a constant vector, provided that $\kappa(s)$ is a solution of equation (2) with $\sigma\neq 0$. Then, translating the origin so that $\mathbf{x}\cdot\mathbf{t}=0$ and $\mathbf{x}\cdot\mathbf{n}=-1/\sigma\left(\kappa^2-\mu\right)$ when $\mathrm{d}\kappa/\mathrm{d}s=0$, which is always possible, one gets $\mathbf{C}=\mathbf{0}$ and obtains expressions (20) for the components of the position vector taking into account the definitions of the tangent and normal vectors (21), as well as the second and third of relations (4). Note that formulas (3) and (20) lead to the remarkable relation

$$r^2(s)=\frac{\varepsilon+\mu^2}{\sigma^2}+\frac{2}{\sigma}\kappa(s) \tag{24}$$

for the magnitude $r(s)=\sqrt{x^2(s)+z^2(s)}$ of the position vector $\mathbf{x}(s)$ rediscovered in [77] (see also [73, 78, 79]).

Thus, the first problem that we have to solve on the way to determine the cylindrical equilibrium shapes of fluid membranes or carbon nanostructures is to find the solutions of equation (2) in analytic form. For that purpose, we express the solutions of its first integral (3) in terms of Jacobi elliptic or elementary functions by means of the roots of the polynomial $P(\kappa)$, the following observations being taken into account.

Depending on the values of the parameters σ, μ and ε, there exist two cases in which the polynomial $P(\kappa)$ attains positive values and hence Eq. (3) has real-valued solutions: (I) the polynomial $P(\kappa)$ has two simple real roots $\alpha,\beta\in\mathbb{R}$, $\alpha<\beta$, and a pair of complex conjugate roots $\gamma,\delta\in\mathbb{C}$, $\delta=\bar{\gamma}$; (II) the polynomial $P(\kappa)$ has four simple real roots $\alpha<\beta<\gamma<\delta\in\mathbb{R}$. In the first case, the polynomial $P(\kappa)$ is nonnegative in the interval $\alpha\leq\kappa\leq\beta$, while in the second one it is nonnegative in the intervals $\alpha\leq\kappa\leq\beta$ and $\gamma\leq\kappa\leq\delta$. It should be noted that the roots of the polynomial $P(\kappa)$ can be expressed explicitly through its coefficients and vice versa, see [29, 73].

According to [29, Corollary 1], only the solutions of the type (I) could give rise to non self-intersecting profile curves.

Let the parameters σ, μ and ε be such that the polynomial $P(\kappa)$ has roots as in case (I), namely, two of them are real ($\alpha<\beta$) and the other two constitute a complex conjugate pair, which can be written in the form

$$\gamma=-\frac{\alpha+\beta}{2}+\mathrm{i}\eta,\qquad \delta=-\frac{\alpha+\beta}{2}-\mathrm{i}\eta$$

where η is a nonnegative real number. In this case, equation (3) has periodic solutions if $\eta\neq 0$ or $\eta=0$ and $(3\alpha+\beta)(\alpha+3\beta)>0$, see [29, Theorem 1].

Let $\eta\neq 0$ and hence the roots of the polynomial $P(\kappa)$ are simple. Denote

$$\lambda = \frac{1}{4}\sqrt{AB}, \qquad k = \sqrt{\frac{1}{2} - \frac{4\eta^2 + (3\alpha+\beta)(\alpha+3\beta)}{2AB}}$$

where

$$A = \sqrt{4\eta^2 + (3\alpha+\beta)^2}, \qquad B = \sqrt{4\eta^2 + (\alpha+3\beta)^2}.$$

Evidently, $A > 0$, $B > 0$, $\lambda > 0$ and $0 < k < 1$. In this case, each solution of Eq. (2) can be expressed by the function

$$\kappa(s) = \frac{(A\beta + B\alpha) - (A\beta - B\alpha)\mathrm{cn}(\lambda s, k)}{(A+B) - (A-B)\mathrm{cn}(\lambda s, k)} \tag{25}$$

which takes real values for each $s \in \mathbb{R}$ and is periodic with least period $T = (4/\lambda)\mathrm{K}(k)$ due to the periodicity of the Jacobi function $\mathrm{cn}(\lambda s, k)$. Here, $\mathrm{K}(\cdot)$ denotes the complete elliptic integral of the first kind. The corresponding slope angle can be written in the form

$$\begin{aligned}\varphi(s) \;&= \frac{\alpha-\beta}{2\lambda\sqrt{k^2 + \dfrac{(A-B)^2}{4AB}}}\arctan\left(\sqrt{k^2 + \frac{(A-B)^2}{4AB}}\,\frac{\mathrm{sn}(\lambda s,k)}{\mathrm{dn}(\lambda s,k)}\right)\\ &+ \frac{(A+B)(\alpha-\beta)}{2\lambda(A-B)}\Pi\left(-\frac{(A-B)^2}{4AB}, \mathrm{am}(\lambda s,k), k\right)\\ &+ \frac{A\beta - B\alpha}{A-B}s\end{aligned} \tag{26}$$

where $\Pi(\cdot,\cdot,\cdot)$ denotes the incomplete elliptic integral of the third kind.

Now, let $\eta = 0$ and $(3\alpha+\beta)(\alpha+3\beta) > 0$. Then, the polynomial $P(\kappa)$ has one double and two simple real roots. The expressions (25) and (26) for the curvature and slope angle, respectively, hold in this case as well, but now the eliptic functions and integrals appearing in these formulas reduce to elementary functions as follows

$$\kappa(s) = \frac{(A\beta + B\alpha) - (A\beta - B\alpha)\cos(\lambda s)}{(A+B) - (A-B)\cos(\lambda s)}$$

$$\varphi(s) = \frac{A\beta - B\alpha}{A-B}s + \frac{8(\alpha-\beta)}{A-B}\arctan\left(\sqrt{\frac{A}{B}}\tan\left(\frac{1}{2}\lambda s\right)\right).$$

It should be remarked that the indefinite integrals $\varphi(s)$ of the foregoing solutions $\kappa(s)$ of Eq. (3) are chosen so that $\varphi(0) = 0$. Moreover, $\kappa(0)$ coincides with the root α of the polynomial $P(\kappa)$, i.e. $\kappa(0) = \alpha$.

Now, having obtained in explicit form the solutions of equation (2), i.e., the curvatures, and the corresponding slope angles, we have completely determined in analytic form the corresponding directrices Γ (up to a rigid motion in the plane) through the parametric equations (20). The closed simple curves among them should meet (see [29, 73]) the transcendental equation (closure condition)

$$\varphi(T)=\frac{(A+B)(\alpha-\beta)}{2\lambda(A-B)}\Pi(-\frac{(A-B)^2}{4AB},k)+\frac{A\beta-B\alpha}{\lambda(A-B)}\mathrm{K}(k)=\pm\frac{2\pi}{n}\cdot \quad (27)$$

Given a closed curve Γ, the geometrical meaning of the integer n appearing in the right-hand side of relation (27) is that it counts out the number of the symmetry axes of the curve Γ, that is the number of the symmetry planes of the deformed fluid membrane or nanotube.

Examples of directrices of cylindrical equilibrium shapes corresponding to solutions to equation (2) of form (25) are presented in Figure 3.

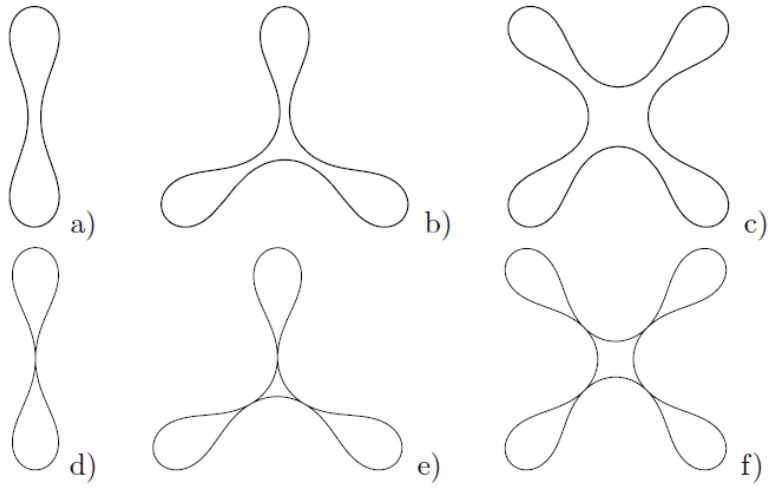

Figure 3. Directrices of some closed cylindrical equilibrium shapes whose curvatures are solutions to equation (2) of form (25) with: a) $\sigma=1$, $\mu=0$, $\varepsilon=0.422$; b) $\sigma=1$, $\mu=1/3$, $\varepsilon=0.814$; c) $\sigma=1$, $\mu=1/3$, $\varepsilon=1.126$. d) $\sigma=5.247$, $\mu=1/2$, $\varepsilon=10.244$; e) $\sigma=21.650$, $\mu=2.955$, $\varepsilon=117.421$; f) $\sigma=51.844$, $\mu=6.712$, $\varepsilon=471.91$.

It is worth noting that Zang *et al.* [80, 81] have compared recently cross-sections of single-wall carbon nanotubes subjected to uniform hydrostatic pressure obtained by numerical solutions of equation (2) and molecular dynamics simulations. As a result, an excellent agreement was observed, see [81, Figure 3]. This observation justifies the applicability of the considered continuum model at least as far as the determination of the cylindrical equilibrium shapes of single-wall carbon nanotubes under hydrostatic pressure is concerned.

3.2 Axially symmetric equilibrium shapes of FM's and CNT's under pressure

This Section is concerned with the analytic representation of a class of axially symmetric surfaces which meet the membrane shape equation (9).

Suppose that a part of an axisymmetric membrane of the considered type admits graph parametrization in a right-handed Cartesian coordinate system with origin O and

axis lines x, y and z. By this we mean that it may be regarded as a surface of revolution obtained by revolving around the z-axis a plane curve Γ laying in the $x\,O\,z$-plane, which is determined by the graph $(x, z(x))$ of a function $z = z(x)$, see Figure 2. For each such surface, the general shape equation (1) reduces to the nonlinear third-order ordinary differential equation (9).

In 1995, Naito *et al.* [25] discovered (see also [2]) that the shape equation for axisymmetric fluid membranes (9) has the following class of exact solutions

$$\sin\psi = ax + b + dx^{-1}, \tag{28}$$

provided that a, b and d are real constants, which meet the conditions

$$\frac{p}{k_c} - 2a^2 c_0 - 2a\left(\frac{c_0^2}{2} + \frac{\lambda}{k_c}\right) = 0, \tag{29}$$

$$b\left(2ac_0 + \frac{c_0^2}{2} + \frac{\lambda}{k_c}\right) = 0, \tag{30}$$

$$b\left(b^2 - 4ad - 4c_0 d - 2\right) = 0, \tag{31}$$

and

$$d\left(b^2 - 4ad - 2c_0 d\right) = 0. \tag{32}$$

Six types of solutions (28) to Eq. (9) can be distinguished on the ground of conditions (29) – (32) depending on the values of the constants c_0, λ and p.

Case A. If $c_0 = 0$, $\lambda = 0$, $p = 0$, then the solutions to Eq. (9) of the form (28) are $\sin\psi = ax$, $\sin\psi = ax \pm \sqrt{2}$ and $\sin\psi = dx^{-1}$, the respective surfaces being spheres, Clifford tori and catenoids.

Case B. If $c_0 = 0$, $\lambda \neq 0$, $p = 0$, then the solutions of the considered type reduce to $\sin\psi = dx^{-1}$ (catenoids).

Case C. If $c_0 = 0$, $\lambda \neq 0$, $p \neq 0$ and $p = 2a\lambda$, then only one branch of the regarded solutions remains, namely $\sin\psi = ax$ (spheres).

Case D. If $c_0 \neq 0$, $\lambda = 0$, $p = 0$, then one arrives at the whole family of Delaunay surfaces corresponding to the solutions of the form

$$\sin\psi = -\frac{1}{2}c_0 x + \frac{d}{x}. \tag{33}$$

Case E. If $c_0 \neq 0$, $\lambda \neq 0$, $p = 0$ and

$$\frac{\lambda}{k_c} = -\frac{1}{2}c_0\left(2a + c_0\right),$$

one gets only solutions of the form $\sin\psi = ax$ (spheres).

Case F. If $c_0 \neq 0$, $\lambda \neq 0$, $p \neq 0$, then four different types of solutions of form (28) to Eq. (9) are encountered: (a) $\sin\psi = ax$ (spheres) if

$$\frac{p}{k_c} = 2a\left(\frac{\lambda}{k_c} + ac_0 + \frac{c_0^2}{2}\right); \tag{34}$$

(b) $\sin\psi = ax \pm \sqrt{2}$ (Clifford tori) if

$$\frac{p}{k_c} = -2a^2 c_0, \quad \frac{\lambda}{k_c} = -\frac{1}{2}c_0\left(4a + c_0\right); \tag{35}$$

(c) solutions of the form (33) (Delaunay surfaces) if

$$p + c_0\lambda = 0; \tag{36}$$

(d) solutions of the form

$$\sin\psi = -\frac{1}{4}c_0\left(b^2+2\right)x + b - \frac{1}{c_0 x}, \tag{37}$$

which take place provided that

$$\frac{p}{k_c} = -\frac{1}{8}c_0^3\left(b^2+2\right)^2, \qquad \frac{\lambda}{k_c} = \frac{1}{2}c_0^2\left(b^2+1\right). \tag{38}$$

Below, following [30], we derive the parametric equations of the surfaces corresponding to the solutions of form (37) to Eq. (9).

First, it is clear that the variable x must be strictly positive or negative, otherwise the right-hand side of Eq. (28) is both undefined and its absolute value is greater than one, which is in contradiction with the sin-function appearing in the left-hand side of this relation.

Next, let us remark that the two last equations in (7) lead to the relation

$$\frac{\mathrm{d}z}{\mathrm{d}x} = \tan\psi, \tag{39}$$

which for the foregoing class of solutions (37) implies

$$\left(\frac{\mathrm{d}z}{\mathrm{d}x}\right)^2 = \frac{\left[b - \dfrac{1}{c_0 x} - \dfrac{1}{4}c_0\left(b^2+2\right)x\right]^2}{1 - \left[b - \dfrac{1}{c_0 x} - \dfrac{1}{4}c_0\left(b^2+2\right)x\right]^2}. \tag{40}$$

In terms of an appropriate new variable t, relation (40) may be written in the form

$$\left(\frac{\mathrm{d}x}{\mathrm{d}t}\right)^2 = -\frac{1}{u^2}Q_1(x)Q_2(x), \tag{41}$$

$$\left(\frac{\mathrm{d}z}{\mathrm{d}t}\right)^2 = \frac{1}{4u^2}\left(Q_1(x) + Q_2(x)\right)^2, \tag{42}$$

where

$$u = -\frac{4}{c_0\left(2+b^2\right)^{3/4}},$$

$$Q_1(x) = x^2 - \frac{4(b+1)}{c_0\left(b^2+2\right)}x + \frac{4}{c_0^2\left(b^2+2\right)}, \tag{43}$$

$$Q_2(x) = x^2 - \frac{4(b-1)}{c_0\left(b^2+2\right)}x + \frac{4}{c_0^2\left(b^2+2\right)}. \tag{44}$$

It should be noticed that the roots of the polynomial $Q(x) = Q_1(x)Q_2(x)$ read

$$\alpha = \frac{2\mathrm{sign}(b)}{c_0\sqrt{b^2+2}}\frac{h-1}{h+1}, \qquad \beta = \frac{2\mathrm{sign}(b)}{c_0\sqrt{b^2+2}}\frac{h+1}{h-1}, \tag{45}$$

$$\gamma = \frac{4b}{c_0\left(b^2+2\right)} - \frac{\alpha+\beta}{2} + i\frac{2\sqrt{2\,|\,b\,|+1}}{c_0\left(b^2+2\right)},$$

$$\delta = \frac{4b}{c_0\left(b^2+2\right)} - \frac{\alpha+\beta}{2} - i\frac{2\sqrt{2\,|\,b\,|+1}}{c_0\left(\varepsilon^2+2\right)},$$

where

$$h = \sqrt{\frac{1+|b|+\sqrt{2+b^2}}{1+|b|-\sqrt{2+b^2}}}. \tag{46}$$

Hence, Eq. (41) has real-valued solutions if and only if at least two of these roots are real and different. Evidently, the roots γ and δ can not be real, but α and β are real provided that $|b| > 1/2$ as follows be relations (45) and (46).

Now, using the standard procedure for handling elliptic integrals (see [82, 22.7]), one can express the solution $x(t)$ of equation (41) in the form

$$x(t) = \frac{2\mathrm{sign}(b)}{c_0\sqrt{b^2+2}}\left(1 - \frac{2h}{h+\mathrm{cn}(t,k)}\right) \tag{47}$$

where

$$k = \sqrt{\frac{1}{2} - \frac{3}{4\sqrt{2+b^2}}}.$$

Consequently, using expressions (43) and (44), one can write down the solution $z(t)$ of equation (42) in the form

$$z(t) = \frac{1}{u}\int\left[x^2(t) - \frac{4bx(t)}{c_0\left(b^2+2\right)} + \frac{4}{c_0^2\left(b^2+2\right)}\right]\mathrm{d}t, \tag{48}$$

that is

$$z(t) = u\left[\mathrm{E}(\mathrm{am}(t,k),k) - \frac{\mathrm{sn}(t,k)\mathrm{dn}(t,k)}{h+\mathrm{cn}(t,k)} - \frac{t}{2} \right], \tag{49}$$

where $\mathrm{E}(\cdot,\cdot)$ is the incomplete elliptic integral of the second kind.

Thus, for each couple of values of the parameters c_0 and b, (47) and (49) are the sought parametric equations of the contour of an axially symmetric surfaces corresponding to the respective solution of the membrane shape equation (9) of form (37).

3.3 Junctions of CNT's to a flat graphene sheet or to other CNT's

The idea of connecting carbon nanotubes can be traced back to the Dunlap's paper [83]. Since then, this idea has attracted much attention due to its feasibility for constructing various nano and micro devices (NEMS and MEMS) that have stimulated theoretical and experimental studies of the junctions' exceptional properties. Three kinds of junctions have been considered: Y junctions, T junctions and junctions between parallel nanotubes (see, e.g., Saito *et al.* [84], Chernozatonskii [85] and the references therein). In the majority of the papers concerning junctions between CNT's, a discrete analysis is applied to determine the junction shapes. Continuum approach to the analysis of the joints between CNT's is presented in [86], and between nanotubes and nanocones – in [87].

The junctions between right circular cylindrical carbon nanotubes and planar graphene sheets are much rarely studied. To the best of our knowledge, this problem is addressed only in the recent papers [86,88,89]. The first paper represents a discrete analysis of the junction using least squares minimization of the difference between the carbon-carbon bond length 1.42Å and the unknown distance of the sheet carbon atoms to the carbon atoms of the tube end. A continuum approach to the same problem is presented in Cox and Hill [89], where Euler's elastica solutions are applied. It should be noted that in the latter paper, the profile curve of the junction is determined extremizing its curvature energy. The suggestion in [89] is that the junction shape could be obtained rotating this curve about the tube axis. However, such an approach does not imply that the curvature energy of the whole junction attains an extremum.

Continuum analysis of the junctions between right circular cylindrical carbon nanotubes and planar graphene sheets or between co-axial carbon nanotubes is presented in [86]. In that paper, the junction is regarded as a two-dimensional surface $\mathcal{S}$ embedded in the three-dimensional Euclidean space $\mathbb{R}^3$ and assumed to exhibit purely elastic bending described by its mean H and Gaussian K curvatures. Its equilibrium shapes are determined by the extremals of the bending energy functional $\mathcal{A}_c$ of Lagrangian density (11) where $c_0 = 0$ and $p = 0$ are assumed. The main goal of [86] is to find approximate solutions to equation (10) determining axisymmetric surfaces that could be considered as possible shapes of the junctions between either two co-axial circular cylindrical carbon nanotubes or one such tube and a planar graphene sheet that is normal to the tube

generatrix.

In the case of a junction between a carbon nanotube and a flat graphene sheet, the value $s = 0$ of the contour corresponds to the points where the tube is attached to the junction and the value $s = L$ corresponds to the points where the junction is attached to the graphene sheet. In the case of a junction between two co-axial carbon nanotubes, the values $s = 0$ and $s = L$ of the contour correspond to the points where the tubes are attached to the junction. In both cases, the boundary conditions for the contour at $s = 0$ are the same and read

$$x(0) = x_1, \qquad z(0) = z_1, \qquad \psi(0) = \frac{\pi}{2}, \qquad \mu(0) = \mu_1,$$

where, x_1 and z_1 are coordinates of a tube endpoint. The conservation law (16) provides a boundary condition for $\mathrm{d}\psi/\mathrm{d}s$ at $s = 0$ of form

$$\left.\frac{\mathrm{d}\psi}{\mathrm{d}s}\right|_{s=0} = \frac{1}{x_1}\sqrt{1 - 2\lambda x_1^2 - 2\eta x_1}. \tag{50}$$

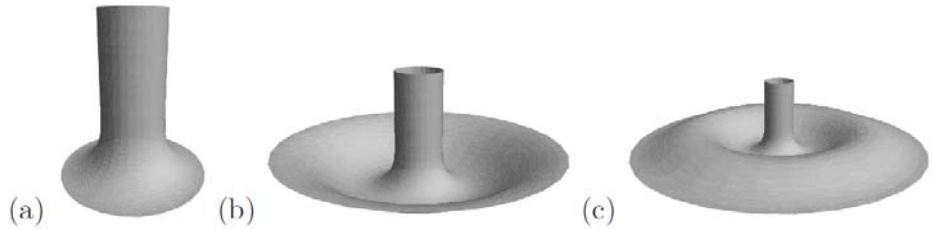

Figure 4. Profile curves and the corresponding junctions between a carbon nanotube and a flat graphene sheet with parameters $\lambda = 1$ and $\mu_1 = 0$. The length of the profile curve is: (a) $L = 2.053$; (b) $L = 5.043$; (c) $L = 8.076$.

To obtain numerical solutions of the foregoing system, a Mathematica® notebook is created using the routine `NDSolve` to solve numerically equations (12), and the routine `ParametricPlot3D` to plot the surface. In all results presented in this Section, $\eta = 0$ in the boundary condition (50) is assumed. The length L of the contour is varied until a continuity of the tangent vector of the junction contour at $s = L$ is achieved. Thus, the boundary condition at $s = L$ is either

$$\psi(L) = 0$$

for a junction between the nanotube and the graphene sheet or

$$\psi(L) = \pm\psi(0)$$

in the case of a junction between two co-axial nanotubes.

Using the aforementioned computational scheme, several examples of junction shapes are obtained. Two possible junctions between a carbon nanotube and a graphene sheet are given in Figure 4. It should be mentioned that two cases of junctions between co-axial carbon nanotubes are possible: either the tubes are on different sides of the junction, or the tubes are on the same side of the junction, see Figure 5.

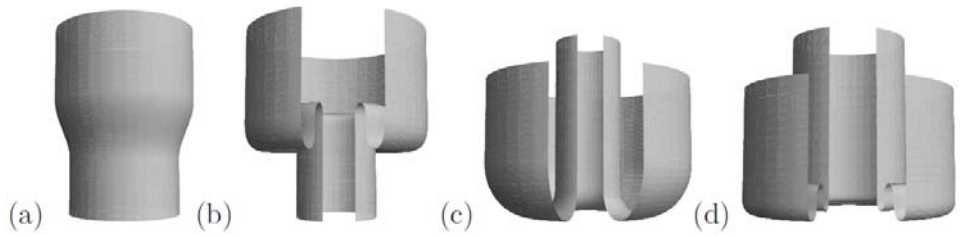

Figure 5. Profile curves and junctions between co-axial nanotubes with parameters: (a) $\lambda = -1$, $\mu_1 = 4.04$, $L = 0.860$; (b) $\lambda = 1/11$, $\mu_1 = -16$, $L = 1.256$; (c) $\lambda = 1$, $\mu_1 = 0$, $L = 1.119$; (d) $\lambda = 1$, $\mu_1 = 67.5$, $L = 0.981$.

To summarize, each of the surfaces on the figures presented herein may be thought of as a possible shape of a junction between a carbon nanotube and a flat graphene sheet or between co-axial carbon nanotubes. It should be noted, that computing the forces and momenta at the edges of the junctions as suggested in [90] we found that they are non-zero, except for the moment at the points where the junction is connected to the graphene sheet. However, no experimental data exist in the literature by now to determine whether these theoretical predictions give realistic results.

3.4 Deformation of injected vesicles adhering onto flat rigid substrates

The success of cell manipulations depends mainly on the mechanical properties of the cell membrane and on the specific way of interaction between the membrane and the other devices. To this end, the determination of the mechanical behaviour of the cells is of primary interest. An apparent approach to this analysis is theoretical determination of certain cell equilibrium shapes and their comparison with experimental observations, typical example being presented by Lu *et al.* [91].

The choice of a model to study the equilibrium shapes of cells depends on the time scale of the phenomena due to the existence of active processes of permeation of matter through the cell membrane [92]. Phenomena that are much faster than the active transfer processes are reasonable to treat using models of deformation that maintain fixed cell volume. In this case, it is widely accepted that the deformation of the cell membrane is localized, the typical examples being Lu *et al.* [91], Boulbitch [93], Bo [94], Sun *et al.* [95], Tan *et al.* [96] and Wan *et al.* [97]). On the other hand, if a phenomenon is much slower that the permeation through the membrane it is reasonable to consider a model that maintains fixed membrane area. In the present study, we consider cells pressed against a rigid wall and are interested in equilibrium shapes that are attained after finishing of the transient transfer of matter through the cell membrane. For this purpose, we employ the simplest model of cells, i.e. closed fluid lipid bilayer membranes (vesicles).

Here, the mechanical behaviour of a vesicle pressed against a rigid wall the vesicle adheres to is examined in the line of the Helfrich spontaneous curvature model. The vesicle membrane is supposed to be inextensible and axisymmetrically deformable. The main task consists in determination of the equilibrium shapes of an initially spherical vesicle adhering to a flat rigid plane subjected to a uniform hydrostatic pressure and a

force exerted onto a given contour. This force is supposed to act along the symmetry axis of the vesicle and to direct inward. Actually, the present model is an extension of the model proposed in [98] in which the cell adhesion has not been taken into account. This is done in the recent work [99].

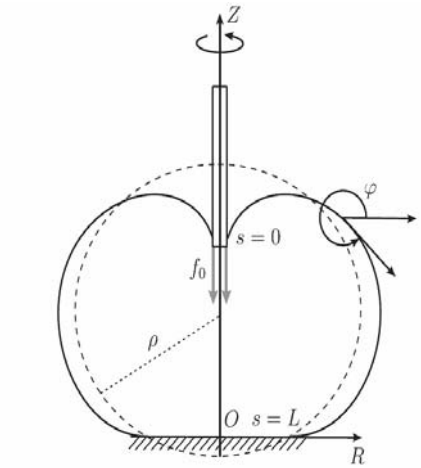

Figure 6. Sketch of an initially spherical cell membrane of radius ρ pressed against the wall. Here, Z-axis is the symmetry axis of the cell, ψ is the slope angle of the profile curve, which is assumed to lie in the ROZ-plane, and f_0 is the magnitude of the force (per unit contour length) acting at the contour $s = 0$.

The membrane is supposed to adhere to a flat rigid plane and to be loaded by the distributed force f_0 and the pressure difference $p = p_o - p_i$, where p_o is the outer solution pressure and p_i is the inner pressure of the vesicle, as is shown in Figure 6. The value $s = 0$ of the arclength variable is assumed to correspond to the point at the profile curve where the external force acts on the cell membrane along the respective contour, which will be denoted by C_0. The value $s = L$ is assumed to correspond to the border of the adhesion area C_L. Denote the external distributed force along the contour C_0 by $f_0 = k_c q_0$ and the pressure on the adhering part of the membrane by p_a. Let us point out that the adhering part of the membrane is flat, and hence $H = 0$ and $K = 0$ there. Then, the shape equation (1) implies $p_a - p_i = 0$ at any point of the adhering part of the membrane. Therefore, the potential energy of the flat part of the membrane adhering to the plane (parametrized by $r(s) = r(L) + L - s$, $z(s) = 0$, $\psi(s) = -\pi$) is

$$2\pi k_c \int_L^{L+r(L)} \mathcal{L}\,\mathrm{d}s = 2\pi k_c \frac{c_0^2 r(L)^2}{4} \tag{51}$$

since along the adhering part of the membrane

$$\alpha\big(L + r(L)\big) - \alpha\big(L\big) = \frac{1}{2} r^2(L).$$

Apparently, the work done by the force f_0 is

$$W_0 = 2\pi r(0) f_0 \big(2\rho - z(0)\big). \tag{52}$$

Taking expressions (51) and (52) into account and accepting that there is a line tension $k_c\sigma_0$ at the contour C_0 due to the membrane – pipette interaction, as well as a line tension $k_c\sigma_L$ at the adhesion border C_L, we arrive at the following expression for the energy stored in the deformed membrane

$$\begin{aligned}\mathcal{A}_{ca} = \mathcal{A}_c + 2\pi k_c \frac{c_0^2 r(L)^2}{4} \\ +2\pi k_c \Big[q_0 r(0)\big(2\rho - z(0)\big) + \sigma_0 r(0) + \sigma_L r(L) - \varpi r^2(L)\Big]\end{aligned}$$

where the adhesion energy per unit area [102, 103] is denoted by $2k_c\varpi$. Then, setting to zero the first variation of the functional $\mathcal{A}_{ca}$ one obtains the system (12) as the Euler-Lagrange equations and the natural boundary conditions (17) take the form

$$\begin{aligned}&\Big[\hat{M}\delta\psi + \hat{\mu}\delta r + \hat{\eta}\delta z\Big]_0^L + Q_0\delta s(0) + Q_L\delta s(L) \\ &+\big[q_0(2\rho - z(0)) + \sigma_0\big]\delta r(0) - q_0 r(0)\delta z(0) \\ &+\left[\left(\frac{1}{2}c_0^2 - 2\varpi\right)r(L) + \sigma_L\right]\delta r(L) = 0,\end{aligned} \tag{53}$$

where

$$\begin{aligned}Q_0 &= \big[q_0\big(2\rho - z(0)\big) + \sigma_0\big]\cos\psi(0) - q_0 r(0)\sin\psi(0) \\ Q_L &= \left[\left(\frac{1}{2}c_0^2 - 2\varpi\right)r(L) + \sigma_L\right]\cos\psi(L).\end{aligned}$$

To analyse the force and momentum balance of the membrane consider its part corresponding to $0 \le s \le s_0$ where $0 < s_0 < L$. The external loads applied to this part of the membrane are the force $\mathbf{f_0} = -f_0\mathbf{j}$ applied at $s = 0$ and the pressure difference P applied at $0 < s < s_0$. Hence, the total external force acting on this part of the membrane reads

$$\mathbf{F}_m(s_0) = -f_0\mathbf{j} + k_c P\int_0^{s_0}\mathbf{N}(s)\mathrm{d}s,$$

and since the unit normal vector $\mathbf{N}(s)$ to the membrane is

$$\mathbf{N}(s) = \left(-\frac{\mathrm{d}z}{\mathrm{d}s}, 0, \frac{\mathrm{d}r}{\mathrm{d}s}\right),$$

the external force simplifies to

$$\mathbf{F}_m(s_0) = k_c P\big(z(0) - z(s_0)\big)\mathbf{i} + \big[-f_0 + k_c P\big(r(s_0) - r(0)\big)\big]\mathbf{j}.$$

Since the part $0 < s < s_0$ of the membrane is in equilibrium, this force is balanced by the

membrane forces at the two ends, namely,

$$\mathbf{F}(s_0) - \mathbf{F}(0) = \mathbf{F}_m(s_0). \tag{54}$$

This formula gives the membrane force distribution at any point $0 < s_0 < L$.

Now, we are prepared to consider the force balance at the point $s = L$. Observing the natural boundary conditions, one finds

$$[[\mathbf{F}]]_{s=L} = \frac{Q_L}{\cos\psi(L)}\mathbf{i}. \tag{55}$$

A simple computation shows that the force within the adhesion area reads

$$\mathbf{F}_a(s) = k_c\left[\left(\frac{c_0^2}{2} - \lambda\right)s + \mu_0\right]\mathbf{i},$$

since the solution of equations (12) in the adhering part of the membrane is

$$\psi(s) = -\pi, \qquad r(s) = L + r(L) - s, \qquad z(s) = 0,$$

$$\hat{\mu}(s) = \mu(s) = \left(\frac{c_0^2}{2} - \lambda\right)s + \mu_0, \qquad \hat{\eta}(s) = \eta(s) = 0,$$

where μ_0 is a constant of integration. Computing the conserved quantity $\mathcal{H}$ given by (16) at a point of the adhering part of the membrane and substituting it in the equality $\mathcal{H} = 0$, μ_0 is determined as

$$\mu_0 = \left(\lambda - \frac{c_0^2}{2}\right)(L + r(L)).$$

Hence,

$$\mathbf{F}_a(L) = k_c\left(\lambda - \frac{c_0^2}{2}\right)r(L)\mathbf{i}.$$

Then, substituting this expression and the limit at $s_0 = L$ of the force (54) in the jump condition (55), one finds the boundary conditions for the components of the membrane force of form

$$\begin{aligned} &\hat{\mu}(L) = \left(\lambda + 2\varpi - c_0^2\right)r(L) - \sigma_L, \\ &\hat{\eta}(L) = 0. \end{aligned} \tag{56}$$

Substituting these expressions in Eq. (54), one obtains the boundary conditions at $s = 0$ as well, namely

$$\begin{aligned} &\hat{\mu}(0) = \left(\lambda + 2\varpi - c_0^2\right)r(L) - \sigma_L - Pz(0), \\ &\hat{\eta}(0) = q_0 - P\left(r(L) - r(0)\right). \end{aligned} \tag{57}$$

The point $s = L$ is free of external momenta and hence a jump condition of form

$$[[M]]_{s=L} = 0, \tag{58}$$

holds at this point. The moment (18) along the adhering part of the membrane is

$$M_a(s) = 2\pi k_c c_0 r(s), \qquad s \in (L, L + r(L)],$$

since $\psi(s) = -\pi$ there. Then, using expression (18) again to obtain the limit value of the bending moment at $s \to L$, $s < L$, the jump (58) reads

$$[[M]]_{s=L} = -2\pi k_c r(L)\left[\frac{\mathrm{d}\psi}{\mathrm{d}s}|_{s=L} + \left(1 + \frac{k_G}{k_c}\right)\frac{\sin\psi(L)}{r(L)}\right]$$

and since $k_c r(L) \neq 0$ it vanishes if

$$\frac{\mathrm{d}\psi}{\mathrm{d}s}|_{s=L} + \left(1 + \frac{k_G}{k_c}\right)\frac{\sin\psi(L)}{r(L)} = 0. \tag{59}$$

We would like to point out the following observations. A boundary condition of form

$$\psi(L) = -\pi \tag{60}$$

is suggested in [100, 101] to ensure the smootness of the membrane shape. In this case, relations (59) – (60) imply another boundary condition of form

$$\left.\frac{\mathrm{d}\psi}{\mathrm{d}s}\right|_{s=L} = 0. \tag{61}$$

Apparently, any other value of $\mathrm{d}\psi/\mathrm{d}s$ leads to a jump of the bending moment at $s = L$.

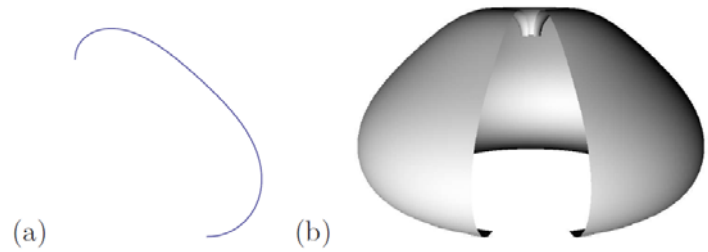

Figure 7. Profile curve (a) and shape (b) of an axisymmetrically deformed initially spherical vesicle adhering to a flat rigid plane with length $L = 1.58$, pressure $P = -50$ and spontaneous curvature $c_0 = 1$.

A boundary condition at the adhesion edge of form

$$\left.\frac{\mathrm{d}\psi}{\mathrm{d}s}\right|_{s=L} = \sqrt{\frac{2\varpi}{k_c}}, \tag{62}$$

is suggested in [100]. However, one should be aware that such boundary condition means a jump in the bending moment at the adhesion border.

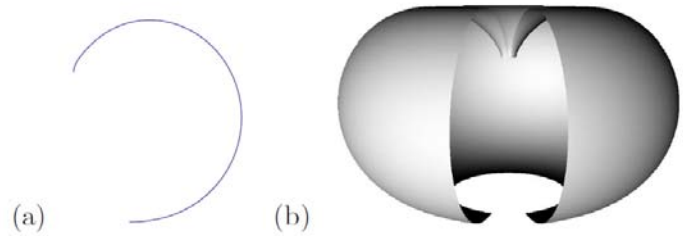

Figure 8. Profile curve (a) and shape (b) of an axisymmetrically deformed initially spherical vesicle adhering to a flat rigid plane with length $L = 2.5$, pressure $P = 25$ and spontaneous curvature $c_0 = 0$.

Explicit analytic parametrization of certain axisymmetric surfaces whose curvature is a solution of the shape equation is presented recently (see [30]). However, it is difficult to find analytical solutions of the nonlinear system (12) due to the specific form of the boundary conditions (56), (57). For that reason, the boundary value problem (12), (56), (57), (60) and (61) is treated numerically using the routine `NDSolve` in Mathematica® (see [102, Sec. 1.6.4]) which is combined with a Maple implementation of the shooting method (package `shoot`, see [103]).

Typical examples of cell membrane shapes are displayed in Figures 7 and 8. The comparison of the membrane shapes in these figures shows up the effect of the external pressure P on the convexity of the equilibrium shape. The profile curves presented in Figure 9 clarify this effect, as well as the effect of the spontaneous curvature on the membrane shape.

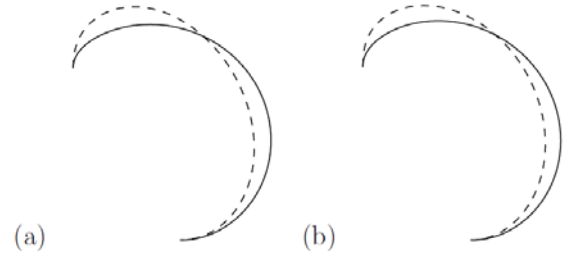

Figure 9. Profile curves of axisymmetrically deformed initially spherical vesicle with length of the great circle 2.7 adhering to a flat rigid plane (bottom) with diameter of the adhesion spot 0.6 and length of the profile curve $L = 1$ (a): $c_0 = 1$, $P = 100$ (solid line) and $P = -100$ (dashed line); (b) $P = 25$, $c_0 = 3$ (solid line) and $c_0 = -3$ (dashed line).

References

1. R. Lipowsky and E. Sackmann (Eds). *Handbook of Biological Physics vol 1*: *Structure and Dynamics of Membranes*. Elsevier, Amsterdam, 1995.
2. Z.-C. Ou-Yang, J.-X. Liu, and Y.-Z. Xie. *Geometric Methods in the Elastic Theory*

of Membranes in Liquid Crystal Phases. World Scientific, Hong Kong, 1999.

3. U. Seifert. Configurations of fluid vesicles and membranes. *Adv. Phys.*, 46:13–137, 1997.
4. P. B. Canham. The minimum energy of bending as a possible explanation of the biconcave shape of the human red blood cell. *J. Theor. Biol.*, 26:61–81, 1970.
5. W. Helfrich. Elastic properties of lipid bilayers: theory and possible experiments. *Z. Naturforsch C*, 28:693–703, 1973.
6. S. Svetina and B. Žekš. Membrane bending energy and shape determination of phospholipid vesicles and red blood cells. *Eur. Biophys. J.*, 17:101–111, 1989.
7. S. Svetina and B. Žekš. Bilayer couple hypothesis of red cell shape transformations and osmotic hemolysis. *Biomed. Biochim. Acta*, 42:86–90, 1983.
8. B. Božič, S. Svetina, B. Žekš, and R. Waugh. Role of lamellar membrane structure in tether formation from bilayer vesicles. *Biophys. J.*, 61:963–973, 1992.
9. L. Miao, U. Seifert, M. Wortis, and H.-G. Dobereiner. Budding transitions of fluid-bilayer vesicles: the effect of area-difference elasticity. *Phys. Rev. E*, 49:5389–5407, 1994.
10. W. Wiese, W. Harbich, and W. Helfrich. Budding of lipid bilayer vesicles and flat membranes. *J. Phys.*: *Condens. Matter*, 4:1647–1657, 1992.
11. Z.-C. Ou-Yang and W. Helfrich. Bending energy of vesicle membranes: general expressions for the first, second, and third variation of the shape energy and applications to spheres and cylinders. *Phys. Rev. A*, 39:5280–5288, 1989.
12. H. S. M. Coxeter. *Introduction to geometry*. Wiley, New York, 2nd edn, 1969.
13. R. Capovilla, J. Guven, and J. A. Santiago. Lipid membranes with an edge. *Phys. Rev. E*, 66:021607–1–7, 2002.
14. Z.-C. Tu and Z.-C. Ou-Yang. Lipid membranes with free edges. *Phys. Rev. E*, 68:061915–1–7, 2003.
15. Z.-C. Tu and Z.-C. Ou-Yang. A geometric theory on the elasticity of bio-membranes. *J. Phys. A: Math. Gen.*, 37:11407–11429, 2004.
16. T. J. Willmore. *Riemannian Geometry*. Oxford, Clarendon, 1993.
17. T. Umeda, Yu. Suezaki, K. Takiguchi, and H. Hotani. Theoretical analysis of opening-up vesicles with single and two holes. *Phys. Rev. E*, 71:011913, 2005.
18. Z.-C. Ou-Yang. Anchor ring-vesicle membranes. *Phys. Rev. A*, 41:4517–4520, 1990.
19. Z.-C. Ou-Yang. Selection of toroidal shape of partially polymerized membranes. *Phys. Rev. E*, 47:747–749, 1993.
20. J.-G. Hu and Z.-C. Ou-Yang. Shape equations of the axisymmetric vesicles. *Phys. Rev. E*, 47:461–467, 1993.
21. H. Naito, M. Okuda, and Z.-C. Ou-Yang. Counterexample to some shape equations for axisymmetric vesicles. *Phys. Rev. E*, 48:2304–2307, 1993.
22. H. Naito, M. Okuda, and Z.-C. Ou-Yang. Polygonal shape transformation of a circular biconcave vesicle induced by osmotic pressure. *Phys. Rev. E*, 54:2816–2826, 1996.

23. I. Mladenov. New solutions of the shape equation. *Eur. Phys. J. B*, 29:327–330, 2002.

24. I. M. Mladenov, M. Ts. Hadzhilazovam P. A. Djondjorov, and V. M. Vassilev. On the intrinsic equation behind the Delaunay surfaces. AIP Conf. Proc., Vol. 1079 (P. Kielanowski and A. Odzijewicz, editors), pp. 274–280, American Institute of Physics, New York, 2008.

25. H. Naito, M. Okuda, and Z.-C. Ou-Yang. New solutions to the Helfrich variational problem for the shapes of lipid bilayer vesicles: beyond Delaunay's surfaces. *Phys. Rev. Lett.*, 74:4345–4348, 1995.

26. V. M. Vassilev and I. M. Mladenov. Geometric symmetry groups, conservation laws and group–invariant solutions of the Willmore equation. In *Geometry, Integrability and Quantization* (I. Mladenov and A. Hirshfeld, editors), pp. 246–265, Sofia, SOFTEX, 2004.

27. B. J. Konopelchenko. On solutions of the shape equation for membranes and strings. *Phys. Lett. B*, 414:58–64, 1997.

28. S. G. Zhang. A complete classification of closed shapes for cylindrical vesicles. *Acta Phys. Sin. (Overseas Edn)*, 6:641, 1997.

29. V. M. Vassilev, P. A. Djondjorov, and I. M. Mladenov. Cylindrical equilibrium shapes of fluid membranes. *J. Phys. A: Math. Theor.*, 41:435201, 2008.

30. P. A. Djondjorov, M. Ts. Hadzhilazova, I. M. Mladenov, and V. M. Vassilev. Beyond Delaunay Surfaces. *J. Geom. Symmetry Phys.*, 18:1–12, 2010.

31. H. Kroto, J. Hearth, S. O'Brien, R. Curl, and R. Smalley. C60: Buckminister-fullerene. *Nature*, 318:162–163, 1985.

32. L. V. Radushkevich and V. M. Lukyanovich. About carbon structures formed during thermal decomposition of carbon oxides at iron surface (in Russian). *Soviet Journal of Physical Chemistry*, XXVI:88–95, 1952.

33. A. Oberlin, M. Endo, and T. Koyama. Filamentous growth of carbon through benzene decomposition. *Journal of Crystal Growth*, 32:335–349, 1976.

34. A. Oberlin, M. Endo, and T. Koyama. High-resolution electron-microscope observations of graphitized carbon-fibers. *Carbon*, 14:133–135, 1976.

35. S. Iijima. Helical microtubules of graphitic carbon. *Nature (London)*, 354:56-58, 1991.

36. S. Iijima, and T. Ichihashi. Single-shell carbon nanotubes of 1-nm diameter. *Nature (London)*, 363:603-605, 1993.

37. D. S. Bethune, C. H. Kiang, M. S. de Vries, G. Gorman, R. Savoy, J. Vazquez, and R. Beyers. Cobalt-catalysed growth of carbon nanotubes with single-atomic-layer walls. *Nature (London)*, 363:605–607, 1993.

38. T. W. Ebbesen, and P. M. Ajayan. Large-scale synthesis of carbon nanotubes. *Nature (London)*, 358:220-222, 1992.

39. N. G. Chopra, L. X. Benedict, V. H. Crespi, M. L. Cohen, S. G. Louie, and A. Zettl. Fully collapsed carbon nanotubes, *Nature (London)*, 377:135–138, 1995.

40. J. Despres, E. Daguerre, and K. Lafdi. Flexibility of graphene layers and carbon nanotubes. *Carbon*, 33(1):87–92, 1995.
41. S. Iijima, C. J. Brabec, A. Maiti, and J. Bernholc. Structural flexibility of carbon nanotubes. *J. Chem. Phys.*, 104(5):2089–2092, 1996.
42. R. S. Ruoff and D. C. Lorents. Mechanical and thermal properties of carbon nanotubes. *Carbon*, 33(7):925-930, 1995.
43. J. Tersoff. New empirical approach for the structure and energy of covalent systems. *Phys. Rev. B*, 37:6991–7000, 1988.
44. D. W. Brenner. Empirical potential for hydrocarbons for use in simulating the chemical vapor deposition of diamond films. *Phys. Rev. B*, 42:9458–9471, 1990.
45. T. Lenosky, X. Gonze, M. Teter, and V. Elser. Energetics of negatively curved graphitic carbon. *Nature*, 355:333–335, 1992.
46. B. I. Yakobson, C. J. Brabec, and J. Bernholc. Nanomechanics of carbon tubes: Instabilities beyond linear response. *Phys. Rev. Lett.*, 76(14):2511–2514, 1996.
47. L. D. Landau and E. M. Lifshitz. *Elasticity Theory*. Pergamon, Oxford, 1986.
48. P. M. Naghdi. Foundations of elastic shell theory. In: *Progress in Solid Mechanics, vol. 4* (I. N. Sneddon and R. Hill, editors), pp. 1–90. North-Holland, Amsterdam, 1963.
49. P. M. Naghdi. The theory of shells and plates. In: *Handbuch der Physik* (S. Flügge and C. Truesdell, editors), pp. 425–640, Springer-Verlag, New York –Heidelberg - Berlin, 1972.
50. F. Niordson. *Shell Theory*. North-Holland, New York, 1985.
51. A. Y. T. Leung and J. L. Kuang Nanomechanics of a multiwalled carbon nanotube via Flugge's theory of a composite cylindrical lattice shell. *Phys. Rev. B*, 71:165415-1-9, 2005.
52. A. Pantano, D. M. Parks and M. C. Boyce. Mechanics of deformation of single- and multi-wall carbon nanotubes. *J. Mech. Phys. Solids*, 52:789–821, 2004.
53. C. Q. Ru. Effective bending stiffness of carbon nanotubes. *Phys. Rev. B*, 62:9973-9976, 2000.
54. C. Q. Ru. Axially compressed buckling of a doublewalled carbon nanotube embedded in an elastic medium. *J. Mech. Phys. Solids*. 49(6):1265–1279, 2001.
55. C. Y. Wang, C. Q. Ru, and A. Mioduchowski. *Int. J. Solids Struct*. Axially compressed buckling of pressured multiwall carbon nanotubes. 40(15):3893–3911, 2003.
56. M. R. Falvo, G. J. Clary, R. M. Taylor, V. Chi, F. R. Brooks Jr., S. Washburn, and R. Superfine. Bending and buckling of carbon nanotubes under large strain. *Nature (London)*, 389:582–584, 1997.
57. J. P. Salvetat, J. M. Bonard, N. H. Thomson, A. J. Kulik, L. Forro, W. Benoit, and L. Zuppiroli. Mechanical properties of carbon nanotubes. *Appl. Phys. A*, 69(3):255–260, 1999.
58. M. M. J. Treacy, T. W. Ebbensen, and J. M. Gibson. Exceptionally hight Young's

modulus observed for individual carbon nanotubes. *Nature (London)*, 381:678–680, 1996.

59. D. W. Brenner, O. A. Shenderova, J. A. Harrison, S. J. Stuart, B. Ni, and S. B. Sinnott. A second-generation reactive empirical bond order (REBO) potential energy expression for hydrocarbons. *J. Phys. Condens. Matter*, 14:783–802, 2002.
60. Z.-C. Ou-Yang, Z. B. Su, and C. L. Wang. Coil formation in multishell carbon nanotubes: competition between curvature elasticity and interlayer adhesion. *Phys. Rev. Lett.*, 78:4055–4058, 1997.
61. Z.-C. Tu and Z.-C. Ou-Yang. Single-walled and multiwalled carbon nanotubes viewed as elastic tubes with the effective Young's moduli dependent on layer number. *Phys. Rev. B*, 65:233407, 2002.
62. Z.-C. Tu and Z.-C. Ou-Yang. Elastic theory of low-dimensional continua and its applications in bio- and nano-structures. *J. Comput. Theoret. Nanoscience*, 5:422–448, 2008.
63. M. Arroyo and T. Belytschko. An atomistic-based finite deformation membrane for single layer crystalline films. *J. Mech. Phys. Solids*, 50:1941–1977, 2002.
64. M. Arroyo and T. Belytschko. A finite deformation membrane based on inter-atomic potentials for the transverse mechanics of nanotubes. *Mechanics of Materials*, 35:193–215, 2002.
65. M. Arroyo and T. Belytschko. Finite crystal elasticity of carbon nanotubes based on the exponential Cauchy-Born rule. *Phys. Ref. B*, 69:115415, 2004.
66. M. Arroyo and T. Belytschko. Continuum mechanics modeling and simulation of carbon nanotubes. *Meccanica*, 40:455–469, 2005.
67. X. Guo, J. B. Wang, and H. W. Zhang. Mechanical properties of single-walled carbon nanotubes based on higher order Cauchy–Born rule. *Int. J. Solids Struct.*, 43(5):1276–1290, 2006.
68. J. B. Wang, X. Guo, H. W. Zhang, L. Wang, and J. B. Liao. Energy and mechanical properties of single-walled carbon nanotubes predicted using the higher order Cauchy-Born rule. *Phys. Rev. B*, 73:115428-1-9, 2006.
69. J. Wu, K. C. Hwang, and Y. Huang. An atomistic-based finite-deformation shell theory for single-wall carbon nanotubes. *J. Mech. Phys. Solids*, 56:279–292, 2008.
70. S. S. Xie, W. Z. Li, L. X. Qian, B. H. Chang, C. S. Fu, R. A. Zhao, W. Y. Zhou, and G. Wang. Equilibrium shape equation and possible shapes of carbon nanotubes. *Phys. Rev. B*, 54:16436–16439, 1996.
71. X. Zhou, J. J. Zhou, and Z. C. Ou-Yang. Strain energy and Young's modulus of single-wall carbon nanotubes calculated from electronic energy-band theory. *Phys. Rev. B*, 62:13692–13696, 2000.
72. X. Zhou, H. Chen, J. J. Zhou, and Z.-C. Ou-Yang. The structure relaxation of carbon nanotube. *Physica B*, 304:86–90, 2001.
73. P. A. Djondjorov, V. M. Vassilev, and I. M. Mladenov. Analytic description and explicit parametrisation of the equilibrium shapes of elastic rings and tubes under uniform hydrostatic pressure. *Int. J. Mech. Sci.*, 53:355–364, 2011.

74. U. Seifert, K. Berndl, and R. Lipowsky. Shape transformations of vesicles: Phase diagrams for spontaneous-curvature and bilayer-coupling models. *Phys. Rev. A*, 44:1182–1202, 1991.

75. F. Jülicher and U. Seifert. Shape equations for axisymmetric vesicles: A clarification. *Phys. Lett. E*, 49:4728–4731, 1994.

76. V. M. Vassilev, P. A. Djondjorov and I. M. Mladenov. Symmetry groups, conservation laws and group-invariant solutions of the membrane shape equation. In: *Geometry, Integrability and Quantization* (I. Mladenov and M. de León, editors), pp. 265–279, SOFTEX , Sofia, 2006.

77. G. Arreaga, R. Capovilla, C. Chryssomalakos, and J. Guven. Area-constrained planar elastica. *Phys. Rev. E*, 65:031801-1-14, 2002.

78. R. Capovilla, C. Chryssomalakos, and J. Guven. Elastica hypoarealis. *Eur. Phys. J. B*, 29:163–166, 2002.

79. J. Guven. Laplace pressure as a surface stress in fluid vesicles. *Journal of Physics A: Mathematical and General*, 39(14):3771–3785, 2006.

80. Ji Zang, A. Treibergs, Y. Han, and F. Liu. Geometric constant defining shape transitions of carbon nanotubes under pressure. *Phys. Rev. Let.*, 92(10): 105501–1–4, 2004.

81. Ji Zang, O. Aldas-Palacios, and F. Liu. MD simulation of structural and mechanical transformation of single-walled carbon nanotubes under pressure. *Commun. Comput. Phys.*, 2(3):451–465, 2007.

82. E. Whittaker and G. Watson. *A Course of Modern Analysis*. Cambridge, Cambridge University Press, 1922.

83. B. Dunlap. Relating carbon tubules. *Phys. Rev. B*, 49(8):5643–5651, 1994.

84. R. Saito, G. Dresselhaus, and M. S. Dresselhaus. Tunneling conductance of connected carbon nanotubes. *Phys. Rev. B*, 53(4):2044–2050, 1996.

85. L. A. Chernozatonskii. *Nanoparticle Res.*, 5:473–484, 2003.

86. P. A. Djondjorov, V. M. Vassilev, and I. M. Mladenov. Junctions between carbon nanotubes and flat graphene sheets or co-axial carbon nanotubes. *Compt. rend. Acad. bulg. Sci.*, 62:805–810, 2009.

87. D. Baowan, B. J. Cox, and J. M. Hill. Modelling the joining of nanocones and nanotubes. *J. Math. Chem.*, 49(2):475–488, 2010.

88. D. Baowan, B. J. Cox, and J. M. Hill. Two least squares analyses of bond lengths and bond angles for the joining of carbon nanotubes to graphenes. *Carbon*, 46:2972–2980, 2007.

89. B. J. Cox and J. M. Hill. A variational approach to the perpendicular joining of nanotubes to plane sheets. *J. Phys. A: Math. Theor.*, 41(12):125203, 2008.

90. Z.-C. Tu. Geometry of membranes. *J. Geom. Symmetry Phys.*, 24:11407–11429, 2011.

91. Z. Lu, P. Chen, H. Luo, J. Nam, R. Ge, and W. Lin. Models of maximum stress and strain of zebrafish embryos under indentation. *Journal of Biomechanics*, 42(5):620–

5, 2009.

92. R. Lipowsky and U. Seifert. Adhesion of vesicles and membranes. *Molecular Crystals and Liquid Crystals*, 202:17–25, 1991.
93. A. Boulbitch. Deflection of a cell membrane under application of a local force. *Physical Review E*, 57(2):2123–2128, 1998.
94. H. Bo. *Towards Automatic Batch Biomanipulation: Study on Robotic Suspended Cell Injection System*. PhD thesis, City University of Hong Kong, 2008.
95. Yu Sun, K.-T. Wan, K. P. Roberts, J. C. Bischof, and B. J. Nelson. Mechanical property characterization of mouse zona pellucida. *IEEE Transactions on NanoBioscience*, 2(4):279–286, 2003.
96. Y. Tan, D. Sun, W. Huang, and S. Cheng. Mechanical modeling of biological cells in microinjection. *IEEE Trans. on NanoBioscience*, 7(4):257–266, 2008.
97. K. Wan, V. Chan, and D. A. Dillard. Constitutive equation for elastic indentation of a thin-walled bio-mimetic microcapsule by an atomic force microscope tip. *Colloids and Surfaces B Biointerfaces*, 27(2-3):241–248, 2003.
98. V. M. Vassilev, K. G. Kostadinov, I. M. Mladenov, A. A. Shulev, G. I. Stoilov, and P. A. Djondjorov. Cell membranes under hydrostatic pressure subjected to micro-injection. AIP Con. Proc. 1340 (Ed. K. Sekigawa et al.), pp. 234–240, 2011.
99. P. A. Djondjorov, V. M. Vassilev and I. M. Mladenov. Deformation of injected vesicles adhering onto flat rigid substrates. *Computers & Mathematics with Applications*, 2012, doi: 10.1016/j.camwa.2012.01.044.
100. U. Seifert and R. Lipowsky. Adhesion of vesicles. *Phys. Rev. A*, 42:4768–4771, 1990.
101. C. Lv, Y. Yin, and J. Yin. Geometric theory for adhering lipid vesicles. *Colloids and Surfaces B: Biointerfaces*, 74:380–388, 2009.
102. S. Wolfram. *The Mathematica Book, Fifth Ed.* Wolfram Media, 2003.
103. D. Meade, B. Haran and E. White. The shooting technique for the solution of two-point boundary value problems. *MapleTech*, 3:85–93, 1996.